



Philipp Koob¹

Technical University of Darmstadt,
Department of Mechanical Engineering,
Institute for Simulation of Reactive Thermo-Fluid
Systems,
Darmstadt 64287, Germany
e-mail: koob@stfs.tu-darmstadt.de

Hendrik Nicolai

Technical University of Darmstadt,
Department of Mechanical Engineering,
Institute for Simulation of Reactive Thermo-Fluid
Systems,
Darmstadt 64287, Germany

Andreas Lindenthal

Technical University of Darmstadt,
Department of Mechanical Engineering,
Institute for Simulation of Reactive Thermo-Fluid
Systems,
Darmstadt 64287, Germany

Frederic Aaron Witkind Hirth

Karlsruhe Institute for Technology,
Institute of Thermal Turbomachinery,
Karlsruhe 76131, Germany

Niklas Bürkle

Karlsruhe Institute for Technology,
Institute of Thermal Turbomachinery,
Karlsruhe 76131, Germany

Thomas Soworka

German Aerospace Center (DLR),
Institute of Propulsion Technology,
Combustor Department,
Cologne 51147, Germany

Ruud L. G. M. Eggels

Rolls-Royce Deutschland Ltd & Co KG,
Blankenfelde-Mahlow 15827, Germany

Carsten Clemen

Rolls-Royce Deutschland Ltd & Co KG,
Blankenfelde-Mahlow 15827, Germany

Rainer Koch

Karlsruhe Institute for Technology,
Institute of Thermal Turbomachinery,
Karlsruhe 76131, Germany

Comprehensive Modeling of the Cause-and-Effect Chain in Aero-Engine Combustor Simulations: From Primary Breakup to Soot Formation

Due to the significant environmental and health impacts, minimizing pollutant emissions, especially soot, is a critical challenge in developing next-generation aero-engines. While predictive soot models in computational fluid dynamics (CFD) are essential for reducing development time and cost, the full simulation of the entire process—from fuel injection and atomization to soot formation and evolution—remains challenging and often involves strong modeling assumptions. To address this challenge, this study combines smoothed particle hydrodynamics (SPH), used to predict liquid fuel atomization, with finite volume method (FVM) large eddy simulations (LES) with advanced combustion and soot models. This approach allows for consistent simulations from fuel breakup to soot formation and enables a detailed investigation of the complex interactions between spray dynamics and soot under engine-like conditions. To accurately capture the primary breakup, the fuel spray particle size distribution (PSD) is sampled from SPH simulations and used to initialize Lagrangian spray particles in the LES, where secondary breakup and evaporation are predicted. The objective of this work is to apply these methods to a single-sector aero-engine combustion chamber operated at elevated pressure and high preheating temperatures, with an aero-engine fuel injector geometry, and to investigate the influence of spray dynamics on soot formation. Comparison with experimental data demonstrates that the applied methods accurately capture the overall flow and combustion characteristics. Spray characteristics sampled from SPH simulations significantly improve the accuracy of mixing and soot formation predictions compared to conventional spray representation approaches. Furthermore, an extended analysis across various operating ranges demonstrates that spray initializations tailored to the respective conditions are essential for achieving accurate pollutant predictions. [DOI: 10.1115/1.4069470]

Keywords: emissions, computational fluid dynamics (CFD), combustion, LES, atomization and sprays, combustor validation

¹Turbo Expo: Turbomachinery Technical Conference & Exposition (GT2025), June 16–20, 2025, GT2025.

¹Corresponding author.

Manuscript received July 6, 2025; final manuscript received July 28, 2025; published online September 24, 2025. Editor: Jerzy T. Sawicki.

Thomas Behrendt

German Aerospace Center (DLR),
Institute of Propulsion Technology,
Combustor Department,
Cologne 51147, Germany

Michael Schroll

German Aerospace Center (DLR),
Institute of Propulsion Technology,
Engine Measurement Systems Department,
Cologne 51147, Germany

Christian Hasse

Technical University of Darmstadt,
Department of Mechanical Engineering,
Institute for Simulation of Reactive Thermo-Fluid
Systems,
Darmstadt 64287, Germany

1 Introduction

Minimizing pollutant emissions remains one of the key challenges in the development of future gas turbines. While soot emissions can be eliminated using carbon-free fuels like hydrogen or ammonia, these fuels can be more easily used in stationary gas turbines. For the aviation sector, where the storage of these carbon-free fuels is especially challenging, sustainable aviation fuels (SAFs) are important for reaching net-zero carbon emissions in the near future. Since soot formation and evolution are very sensitive to mixture formation and, hence, also to the fuel feedstock, improved soot models embedded into high-fidelity computational fluid dynamics (CFD) are essential for the development of future sustainable aero-engines.

Although soot model development has been an ongoing topic, its primary focus has been on academic setups rather than on engine-relevant, multiphase configurations [1]. While semi-empirical soot models, such as the two-equation soot model [2], offer low computational costs, they are only accurate under the specific conditions for which they were developed, greatly restricting their broader applicability. With increasing available computational resources, more sophisticated approaches such as methods of moments or sectional methods have become feasible not only for simplified configurations but also for application-relevant setups [3,4]. These models are developed and improved in academic configurations and subsequently applied to cases with increased complexity. For the simulation of an aero-engine combustion chamber, the full chain of physical processes involved, from fuel injection and atomization to mixture formation, initial soot particle formation in the primary combustion zone, and subsequent soot evolution in the postflame zone must be captured with adequate models. Soot formation under engine-relevant conditions was successfully investigated for full-scale aero-engine combustors with large eddy simulations (LES) in recent works [3–5]. However, in these works, simple models for the fuel spray breakup were applied.

The mixture formation in aero-engine combustors is determined by the breakup and evaporation of the liquid fuel. In modern aircraft engines, the fuel is usually injected into the combustion chamber through airblast atomizers [6]. The liquid fuel film is spread over a prefilmer surface, pushed to the trailing edge by the high-velocity bypassing airflow, and starts to break up after detaching. The breakup process remains poorly understood, as experimental investigations near the atomizer edge are challenging due to the high density of the liquid fuel spray, and detailed numerical simulations of the two-phase flow are particularly expensive. Studies are often restricted to simplified, academic configurations, such as a planar atomizer [7], which cannot represent all phenomena of circular aircraft atomizers operated at high temperatures and

elevated pressure. Although first numerical approaches to simulate the fuel breakup of realistic aircraft airblast atomizers were presented by Dauch et al. [8] and Warncke et al. [9], including these detailed methods directly in the full combustor simulation remains prohibitively expensive. To reduce computational costs, the atomization process is therefore often excluded, and the fuel spray is initialized with a presumed particle size distribution, e.g., following Rizk and Lefebvre [10] by applying a modified Rosin–Rammler distribution. The subsequent spray evolution is then modeled with a Lagrangian particle tracking approach. A first attempt to use detailed spray initializations generated with smoothed particle hydrodynamics (SPH) in reactive LES of a combustion chamber was recently presented by Okraschevski et al. [11] for the numerical simulation of high altitude relight at subidle operation. The results highlight the potential of coupling these methods to further improve the accuracy of numerical simulations.

This idea serves as the starting point for this study and is further extended to better understand the interaction of detailed spray dynamics and soot formation. This work explores the coupling of SPH spray breakup simulations and reactive LES and its importance for reliable modeling of soot formation under realistic operating conditions. By varying the sampling strategy of spray droplet particle size distributions (PSDs) retrieved from SPH simulations in reactive LES, the influence on the mixture and soot formation is studied in a single-sector aero-engine model combustor featuring an aero-engine fuel injector, which is investigated experimentally using laser-optical measurement methods. The objectives of this work are:

- Validation of the coupled simulation approach with available experimental data
- Analysis of the influence of the spray initialization on soot predictions
- Assessment of the required spray details to predict emissions over the entire operating range

The remaining paper is structured as follows: First, the experimental setup of the investigated single-sector combustor and the measurement methods are presented in Sec. 2. This is followed by the description of the numerical methods and the computational setup in Sec. 3. Details on the spray breakup modeling with SPH and the coupling to the reactive LES are given in Sec. 4. Thereafter, in Sec. 5, the results are presented and discussed. Finally, the conclusions of this study are given in Sec. 6.

2 Single Sector Configuration

2.1 Experimental Setup. The experimental campaign was conducted in the Single Sector Combustor (SSC) test facility of

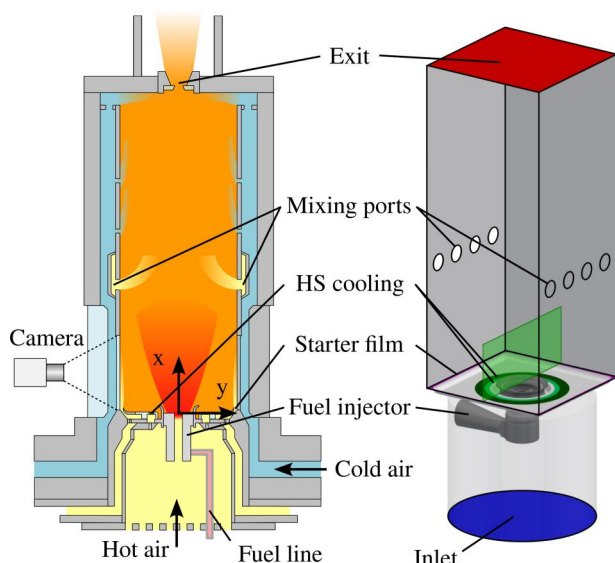


Fig. 1 Experimental setup and CFD domain. The location of the measurement plane in the CFD domain is highlighted at the bottom of the combustor (green). (Color version online)

Table 1 Operating conditions

	Case A	Case B	Case C	Case D
Pressure in bar		9.3		
Temperature in K		603		
Fuel mass flow in g s^{-1}	11.5	9.3	7.2	5.7

the DLR Institute of Propulsion Technology in Cologne, Germany. The test rig is specifically designed for laser-optical investigations of the burner near field under realistic operating conditions and was used in the past for various studies of the soot formation process in rich-quench-lean burners for aero-engine applications, e.g., Ref. [12]. The test rig and measurement techniques are also described in detail in Ref. [12]; only the main features are briefly outlined here.

The SSC provides optical access to the reacting flow field from three sides through planar fused silica windows. One side is equipped with a metal liner that holds a hydrogen torch igniter. A preheated starter film is applied along the windows in the primary zone on the hot gas side, cooling the windows and preventing seeding particles from settling on them during particle image velocimetry (PIV) measurements. The majority of the preheated air bypasses the primary zone and enters the metal flame tube 103 mm downstream of the heat shield through opposing mixing ports (see Fig. 1). The air split is controlled by critical nozzles and is nominally set as follows: 62.2% for mixing ports, 15.9% for starter film, and 21.9% for burner including heat shield cooling. For PIV measurements, the starter film air split was increased to around 30% to effectively prevent particle deposition on the liner windows. This adjustment is expected to have a negligible impact on spray preparation and soot formation in the burner's near field. Most of the cooling air is fed into the combustor just upstream of the outlet nozzle, where it is also used to control the desired combustor backpressure. The temperature and pressure upstream of the burner are set to 603 K and 9.3 bar. The burner pressure drop is held constant at 3.1% and the fuel mass flow is varied to study soot formation at different air-fuel ratios. The operating conditions are summarized in Table 1. The kerosene surrogate D70² is used for the tests. It has similar properties to Jet A-1, but with a lower aromatic content (max. 2000 ppm). This reduces signal trapping and laser absorption and extends the applicability of the optical measurement

techniques to a wider range of fuel-rich test conditions. An assessment of the differences in soot formation of Jet A-1 and D70 in a different test rig showed that the flame structure and soot distribution remain nearly unchanged between both fuels. The level of soot, however, is found to be reduced with the lower aromatic fuel D70. Similar trends were observed by Hassa et al. [13], who compared Jet A-1 with different low-aromatic biofuel blends.

2.2 Measurement Methods. The application of optical measurement techniques in fuel-rich flames presents several significant challenges, including high flame luminosity, strong gradients in temperature and gas composition, as well as UV laser and signal trapping by soot particles. The experimental setup has been adopted to address these challenges, as described in Refs. [12,14].

The flow field is measured by PIV using a dual camera setup. This allows individual exposure of each camera in the submicrosecond range and reduces saturation caused by the high flame luminosity [15]. Seeding particles (porous silica spheres) are introduced only into the burner air mass flow during the PIV measurements. An Nd:YAG laser (532 nm, 100 mJ, 25 Hz) is used to generate a laser light sheet over the height of the optically accessible region (see measurement plane in Fig. 1). According to Ref. [12], the accuracy of the flow field obtained by the described PIV measurements is in the range of 5–10%.

The location of the heat release zones is determined experimentally by the radiation of the electronically excited OH radical. It is captured by a UV-sensitive camera with a bandpass filter ($317 \text{ nm} \pm 10 \text{ nm}$). The detected signal on each pixel corresponds to the line-of-sight integral over the combustor depth. A series of 800 frames is acquired at 10 Hz to create a time-averaged image. Assuming rotational symmetry, the average OH* chemiluminescence distribution in the central plane is reconstructed using the onion-peeling method.

The soot volume fraction in the reacting flow field is quantified by laser-induced incandescence (LII). A laser light sheet (1064 nm, 60 mJ, 10 Hz) heats up the soot particles. A camera perpendicular to the laser light sheet captures the spectrally filtered ($450 \text{ nm} \pm 10 \text{ nm}$) incandescence signal. The camera is operated in double-frame mode, which allows the LII signal to be corrected for background luminosity on a single-pulse basis. The LII signal is calibrated with a laser absorption measurement according to Refs. [14,16] with a Nd:YAG laser (532 nm, <1 mJ, 10 Hz) 1 μs before the LII laser pulse. The uncertainty of the LII measurements is about 10% and is mainly dictated by the laser absorption measurement [12].

3 Numerical Methods and Setup

To simulate this engine-relevant configuration with CFD, all physical processes have to be modeled appropriately, as the weakest model will determine the overall error. In this work, a finite volume method (FVM) is used for the reacting simulation of the entire combustion chamber, and smoothed particle hydrodynamics (SPH) is applied for the detailed simulations of spray breakup in the fuel injector. In the following, the two applied CFD methods and the corresponding numerical setups are presented.

3.1 Reactive Large Eddy Simulations Solver. All LES of the combustion chamber are performed using the Rolls-Royce CFD solver PRECISE-UNS [17]. The cell-based finite volume solver tailored to the simulation of aero-engine combustion chambers solves the Favre-filtered Navier–Stokes equations in the low Mach number formulation. Second-order central differences are applied to discretize the pressure and the velocity. All scalar equations are discretized using a second-order variation diminishing scheme [18]. The equations are advanced in time using second-order backward differences. The σ -model by Nicoud et al. [19] is used for the modeling of the unresolved subgrid fluxes.

3.1.1 Combustion Model. The gas-phase chemistry is modeled with a tabulated chemistry approach [20] using a detailed kinetic

²Testbenzin D70, provided by Staub & Co. - Silbermann GmbH, Germany

mechanism for kerosene surrogates specialized in the formation of soot precursors [21]. A combination of 52 vol. % dodecane ($C_{12}H_{26}$), 15.8 vol. % iso-octane (C_8H_{18}), 12.1 vol. % cyclohexane (C_6H_{12}), and 20.1 vol. % trimethylbenzene (C_9H_{12}) is used for the representation of the fuel. The applied kinetic mechanism was optimized for this surrogate composition, and both were previously applied together for simplified [22] and realistic configurations [4]. Because the flame properties and soot distribution of D70 and Jet A-1 are comparable, it is expected that the difference in the fuel will only affect the overall soot level. Three hundred premixed flamelets inside the flammability limits are used for the tabulation, and the progress variable $Y_C = Y_{CO_2} + Y_{CO} + Y_{H_2O} + Y_{H_2}$ is used. The presumed probability density function (PDF) approach is applied to account for the unresolved turbulence chemistry interaction, adding the variances of the progress variable Y_C and the mixture fraction Z to the set of control variables. The presumed PDFs are a beta function for the mixture fraction and a three-delta peak for the progress variable [23]. The assumption of a three-delta peak might lead to errors when the variances become large, such as in Reynolds-averaged Navier–Stokes (RANS) or very coarse LES. Since the magnitude of the variances in the current LES is low due to the very fine grid in the regions of high reactivity, the influence is minor in the current study. Following Ref. [24], the scalar dissipation rate in the variance equation is modeled by assuming that the scalar dissipation rates of the fluctuations are linked to a turbulent mixing time τ_t with a linear relaxation assumption

$$\rho D \frac{\partial c''}{\partial x_i} \frac{\partial c''}{\partial x_j} \approx \bar{\rho} C_\sigma \frac{\tilde{c}''^2}{\tau_t} = C_\sigma \frac{\mu_t}{Sc \Delta^2} \tilde{c}''^2 \quad (1)$$

where C_σ is a proportionality constant of the order of unity, $Sc = 0.7$ the turbulent Schmidt Number and Δ the filter size of the LES. The reaction term \tilde{c}''^2 measures the correlations between scalar fluctuations and the reaction rate and is provided by the probability density function:

$$\begin{aligned} \overline{c'' \dot{c}} &= \overline{(c - \tilde{c}) \dot{c}} = \int_0^1 (c^* - \tilde{c}) \dot{c}_c(c^*) p(c^*) dc^* \\ &= \overline{\dot{c}_c c} - \overline{\dot{c}_c \tilde{c}} \end{aligned} \quad (2)$$

For the tabulation, 400 points for Z , 101 points for Y_C , and 10 points for the variances \tilde{Z}''^2 and $\tilde{Y}_C''^2$ are used. A nonequidistant spacing is applied to the mixture fraction and the variances to minimize interpolation errors during table access.

3.1.2 Soot Model. The formation and evolution of soot particles are modeled with the split-based extended quadrature method of moments (S-EQMOM) [25]. This model approximates the unknown soot number density function (NDF) $n(x_i, t, \xi)$ by a set of two coupled sub-NDFs $n_{s_l}(x_i, t, \xi)$. x_i is the i -th component of the coordinate vector, t the time, and s_l the index of the sub-NDF. All particles are assumed to be spherical. Therefore, the internal coordinate vector ξ consists only of the soot particle volume V . By solving transport equations for the three lower-order moments m_k , $k = 0, 1, 2$, of each sub-NDF, the evolution of soot is modeled

$$\frac{\partial \bar{m}_k(\mathbf{x}, t)}{\partial t} + \frac{\partial \tilde{u}_i \bar{m}_k(\mathbf{x}, t)}{\partial x_i} = \bar{m}_k \quad (3)$$

$$\dot{m}_k = \dot{w}_{nuc,k} + \dot{w}_{coa,k} + \dot{w}_{con,k} + \dot{w}_{HACA,k} + \dot{w}_{ox,k} \quad (4)$$

with the i th velocity component u_i and the source term \dot{m}_k . Nucleation of primary soot particles from the soot precursor Pyrene ($C_{16}H_{10}$), coagulation, surface growth through condensation, the hydrogen abstraction/acetylene addition (HACA) mechanism, and soot oxidation with OH and O_2 are covered in the source term. The different processes included in the model are described in detail in the work of Salenbauch et al. [25].

3.1.3 Coupling of the Soot and the Chemistry. The mass transfer from the gaseous phase to the solid soot phase through

nucleation and the slow polycyclic aromatic hydrocarbon's (PAHs) chemistry is accounted for by introducing an additional PAH transport equation [26]:

$$\frac{\partial \bar{\rho} \tilde{Y}_{PAH}}{\partial t} + \frac{\partial \bar{\rho} \tilde{u}_i \tilde{Y}_{PAH}}{\partial x_i} = \frac{\partial}{\partial x_i} \left[\bar{\rho} (D_e) \frac{\partial \tilde{Y}_{PAH}}{\partial x_i} \right] + \bar{\omega}_{PAH} \quad (5)$$

ρ is the density and D_e is the effective diffusion coefficient, composed of the laminar and turbulent contributions. The PAH source term $\bar{\omega}_{PAH}$ is split into three parts: A chemical production term $\bar{\omega}_{PAH}^+$, a chemical destruction term $\bar{\omega}_{PAH}^-$ linear dependent on Y_{PAH} , and a consumption term modeling the mass transfer from the gas phase to the solid soot phase $\bar{\omega}_s$, quadratic to Y_{PAH} :

$$\bar{\omega}_{PAH} = \bar{\omega}_{PAH}^{+T} + \bar{\omega}_{PAH}^{-T} \left(\frac{\tilde{Y}_{PAH}}{\tilde{Y}_{PAH}^T} \right) + \bar{\omega}_s^T \left(\frac{\tilde{Y}_{PAH}}{\tilde{Y}_{PAH}^T} \right)^2 \quad (6)$$

Quantities denoted with the superscript T are stored in the flamelet manifold. Recent studies have demonstrated the soot models suitability for modeling soot formation under conditions relevant to aero-engine applications [4,22].

In the confined combustion chamber of an aero-engine, the impact of radiative heat transfer is less important than in an open flame configuration [27,28]. The heat of the flame cannot leave the combustor and is mostly reflected from the walls into the combustor, and the heat absorbed by the walls is reintroduced to the combustion chamber through the wall cooling air. The overall impact of radiative heat transfer on soot formation is expected to be only marginal, and it is, therefore, neglected for this study.

3.1.4 Lagrangian Spray Model. The liquid spray is modeled using a Lagrangian particle tracking approach. The Lagrangian spray solver is running on separate cores to improve the scalability of the coupled Euler-Lagrangian solver [29]. Sec. 4 discusses the determination of the starting positions for these Lagrangian particles in detail.

3.2 Numerical Setup. Figure 1 shows the domain with colored boundary conditions and the position of the experimental measurement plane in green next to the experimental setup. Preheated air is supplied to a plenum upstream of the burner and flows through the fuel injector into the combustion chamber. Additional air enters the primary zone of the combustor through the heat shield (HS) cooling holes and the starter film at the edges of the heat shield. While the starter film is modeled with a regular inflow boundary condition, the HS cooling air is modeled with an effusion boundary condition. The small holes are replaced by a patch with uniform mass flow while an additional momentum source term ensures the correct momentum of the cooling airflow. To represent the tangentially and radially aligned holes of the real heat shield, two separate effusion boundary conditions with tangential and radial inflow directions are implemented. The liquid fuel spray is injected into the combustion chamber with a fuel mass flow of $\dot{m}_f = 11.5 \text{ gs}^{-1}$ (Case A), as detailed in Sec. 4.2. Downstream of the primary combustion zone, secondary air is introduced into the combustion chamber through mixing ports, resulting in fast mixing and quenching of the rich burned products. All walls are assumed to be adiabatic.

The domain is discretized by approximately 16 million cells using an octree-based algorithm. The resulting mesh consists mainly of hexahedral cells with polyhedrons towards boundaries and the transition between cell sizes. The maximum cell size is 0.5 mm in the primary zone and 0.25 mm in the injector. A constant time-step is chosen, and the resulting Courant-Friedrichs-Lewy number is below 0.3 in the combustion chamber and below 0.7 in the refined region of the fuel injector. The quality of the LES is estimated by applying the IQ_v criterion by Celik et al. [30]. This results in values $> 80\%$ in all regions of interest of the combustion chamber, which is considered a

good quality LES. Simulations are conducted at the operating conditions given in Table 1 of the SSC for all four fuel mass flows.

4 Spray Modeling

In this section, details on the modeling of the spray breakup and the coupling of SPH with the full combustor simulation are presented.

4.1 Primary Breakup Solver. The SPH method [31] is a mesh-free approach in which the fluid is discretized into a set of Lagrangian particles of constant mass. The proprietary in-house SPH-code “turbo-SPH” [11,32,33] is used for detailed simulations of fuel atomization in the investigated injector.

This study employs a weakly compressible SPH formulation [34], calculating the pressure field via the Cole equation of state [35] with an added background pressure. The numerical schemes used are detailed in Okraschevski et al. [11], and centrifugal forces of the swirled airflow are modeled following the approach by Dauch et al. [36].

A particle size of $5\ \mu\text{m}$ is used to discretize the computational domain of the SPH simulations. Previous studies have shown that this resolution is sufficient to reproduce the main characteristics of the spray breakup and the particle size distribution, as shown by Braun et al. [32] for a planar atomizer with a similar Weber number to the injector applied in this study. Additionally, the volumetric weighted particle size distribution sampled from a simulation with a resolution of $2.5\ \mu\text{m}$ shows very similar results to the $5\ \mu\text{m}$ resolution. Since discretizing the entire combustor with this resolution is prohibitively expensive, the computational domain is restricted to a stream tube around the primary atomization zone following the procedure described in Refs. [11,37]. Slip conditions are applied to the streamline walls, as indicated in Fig. 2, and velocity profiles at the inlet boundaries are interpolated from a preceding RANS simulation of the complete combustor. Spray statistics are sampled inside a 1.5mm wide measuring area following the methodology presented in Ref. [11]. The sampling position is chosen far enough downstream of the atomizer edge to ensure complete primary atomization. Only clusters with at least four SPH particles are considered droplets, leading to a minimal diameter of $\approx 10\ \mu\text{m}$.

4.2 Spray Interface. Although a direct coupling of both methods would be desirable as it contains the highest detail of the spray droplet characteristics, the involved temporal and spatial scales differ significantly between SPH and FVM. Therefore, instead of a direct coupling, an iterative indirect approach is selected, as depicted in Fig. 3. The general flow characteristics and boundary conditions required for the simulation of the fuel spray breakup are extracted from an initial RANS simulation of the entire combustion chamber. Detailed spray droplet PSDs are sampled from the following SPH simulation of the fuel breakup and used as spray

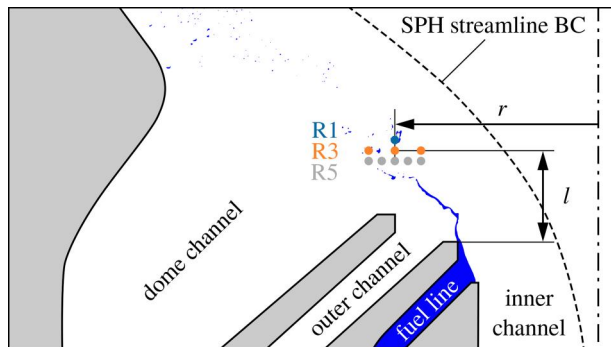


Fig. 2 Initialization positions of the spray PSD in the injector and spray breakup simulated with SPH

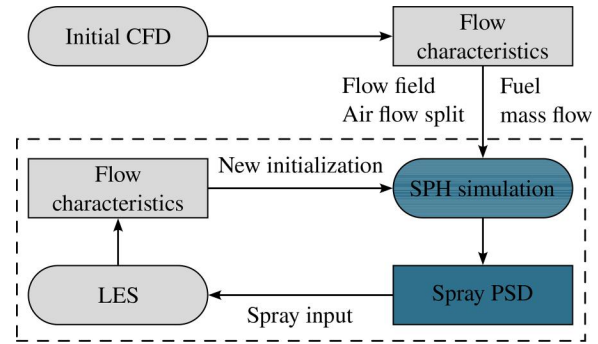


Fig. 3 Workflow of the coupling of SPH and LES

boundary conditions in the reactive LES of the entire combustor. To mitigate the potential influences of the initial simulation on the spray dynamics, the flow field as predicted by the LES should be used to recalculate the spray breakup in an iterative process until the spray dynamics and resulting flow field converge. The necessity and number of iterations will largely depend on the initial spray estimate used in the preliminary RANS simulation and will be discussed in the result section. The fuel spray in the LES is initialized at a prescribed location with a specific spray PSD by providing the droplet diameters and the corresponding particle number density. The location and mean velocity of the spray is set according to the SPH simulations. Since the starting positions of the spray droplets in the LES are not obvious, this influence is investigated in this study by applying different initialization strategies. Transient conditions are accounted for by superimposing the initial droplet velocity with local turbulent fluctuations. If not stated differently, the initialized distribution is assumed to correspond to the distribution after the primary spray breakup. A secondary breakup model [38] is applied to model the subsequent spray evolution, and evaporation is modeled using a steady-state evaporation model [39].

4.2.1 Spray Boundary Conditions. Different fuel spray initializations are applied in this study to investigate their influence on soot predictions. The distributions are sampled from the detailed SPH spray breakup simulations and initialized at the sampling distance l from the atomizer edge of the fuel injector. Around 9400 droplets are sampled from the SPH, and their particle size over the normalized radial position is plotted in Fig. 4 on the left. The normalization length D corresponds to one-tenth of the inner diameter of the heat shield. Most particles are found at around $1D$, and sizes between $10\ \mu\text{m}$ and $130\ \mu\text{m}$ are observed. For the simplest initialization, the PSD of all particles is calculated, and the velocity and radial position r of the initialized particles corresponds to the mean value of all spray droplets (R1). The level of detail included in the initialization is increased by including additional information on the radial distribution. Therefore, the spray droplets are sampled over different radial positions r in the first step, and the corresponding PSD is initialized with the respective mean velocity. The sampling for case A is shown as an example for three radial positions (R3) in Fig. 4,

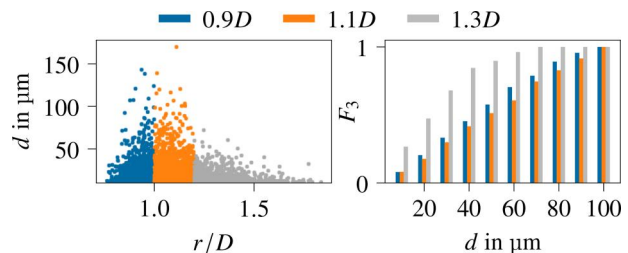


Fig. 4 Spray droplets for case A sampled over three radial positions (left) and the resulting normalized cumulative volume-based particle size distribution (right) for R3

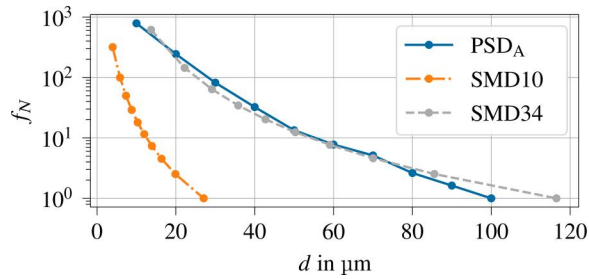


Fig. 5 Normalized number-based spray particle size distribution for the distribution sampled from the SPH simulation and two modified Rosin–Rammler distributions with different d_{32}

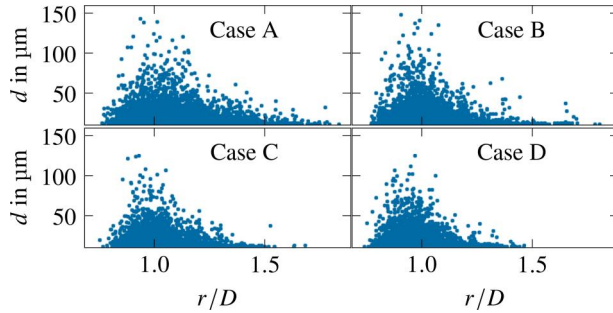


Fig. 6 Distribution of the spray droplet size over the radial position sampled from SPH simulations for the respective operating conditions

together with the resulting normalized cumulative volume-based spray PSD. While the two inner radial sampling positions of $0.9D$ and $1.1D$ have very similar PSDs, the outer position at $1.3D$ is only composed of droplets smaller than $70\ \mu\text{m}$. Although droplets are found further outside, their total number is small, and the mean radial position is still close to $1.3D$. Each radial position is initialized with the corresponding mean particle velocity. The same procedure is repeated with five radial positions (R5) by adding initialization at $r = 1.0D$ and $r = 1.2D$. Two additional distributions sampled from a modified Rosin–Rammler distribution [10] are applied as a reference. The second distribution with a Sauter mean diameter (SMD) $d_{32} = 34\ \mu\text{m}$ (SMD34) is fitted to the distribution obtained from the SPH simulation of Case A. The second distribution with a smaller SMD of $d_{32} = 10\ \mu\text{m}$ (SMD10) is used to represent a spray distribution after secondary breakup. Therefore, no secondary breakup model is required for this distribution. The normalized number-based PSDs are shown in Fig. 5.

For the investigation of all operating points (case A–D), case-specific PSDs are sampled from the respective SPH simulations. The distributions of the droplets over the radial positions for all cases are shown in Fig. 6. In all cases, most droplets are found at around $1D$. Increasing the fuel mass flow leads to increased radial spreading of the droplets and larger maximum droplet sizes. The mean radial position moves from $1D$ for case D to $1.08D$ for case A.

5 Results and Discussion

LES with the S-EQMOM soot model are performed for all previously presented spray initializations. In the following of this section, the results are presented and analyzed. First, the general flow characteristics are presented, and results with different spray initializations are compared to the experimental reference data. Afterward, the influence of the spray dynamics on soot formation is studied, and, finally, the impact of different operating conditions on the spray dynamics soot interaction is investigated.

5.1 Global Flow Characteristics. To understand the general flow characteristics in the region of the combustion chamber relevant to this study, Fig. 7 shows the instantaneous (left) and averaged (right) fields of the normalized axial velocity u_n , the equivalence ratio ϕ , the normalized temperature T_n , and the normalized soot volume fraction $f_{v,n}$ in the center of the primary zone, corresponding to the experimental measurement plane, for the base case A. The swirled flow opens up after entering the combustion chamber, and a recirculation zone is formed at the center. The additional fresh air entering through the starter film is visible at the combustor walls, where high velocities are paired with low temperatures and an equivalence ratio of zero, especially visible in the instantaneous fields. The flame is burning in the central lower part of the combustor, where high temperature gradients are observed. As expected, the highest temperatures are observed at the stoichiometric mixture fraction and in the recirculation zone. While the main branches of the flow consist of a rich mixture, the recirculation zone has a leaner composition due to the additional air introduced by the downstream mixing ports. Soot is predominately present in the rich regions, and locally increased values correlate with a higher local equivalence ratio. In the near-wall region, where the hot burned products are quenched with fresh air from the starter film, soot is also present in lean mixtures. Additionally, local, instantaneous pockets of the soot volume fraction are significantly higher than the temporal mean, highlighting the strong fluctuations and transient behavior of the turbulent flame and its interaction with the soot formation mechanism. In the following, the CFD setup is validated against the available experimental data in the primary combustion zone by means of the velocity fields and flame position. Figure 8 shows the comparison of the normalized mean velocity components \bar{u}_n and \bar{v}_n from the experiments with simulation results. The maximum value of all plots is used for the normalization. Simulation results are shown for the reference distribution and the distribution sampled at one point (R1). Both simulations capture the central recirculation zone and the global flow characteristics well. Note that the velocity measurement near the fuel injector with PIV is obstructed by the present liquid fuel droplets. Smaller droplets, comparable in size to the seeding particles, cannot be distinguished due to their similar light-scattering properties. Larger droplets and filaments scatter light differently but cause overexposure in this region. Consequently, velocity measurements in this area are unreliable. The differences in the recirculation zone between the simulation and experiment for the lowest axial position are attributed to these measurement difficulties and the corresponding measurement points are marked in gray. The high axial velocity near the wall at lower positions, induced by the starter film, is observed in

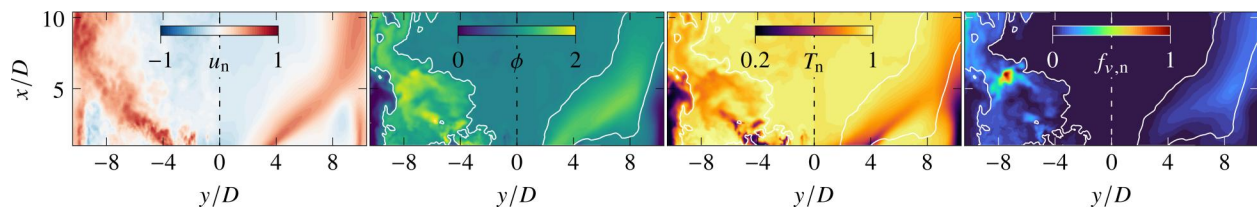


Fig. 7 Contour of the instantaneous (left) and mean (right) flow field. From left to right: normalized axial velocity, equivalence ratio, normalized temperature and normalized soot volume fraction. Normalization is achieved by dividing with the respective local maximum value. The stoichiometric mixture fraction is marked with a white isoline.

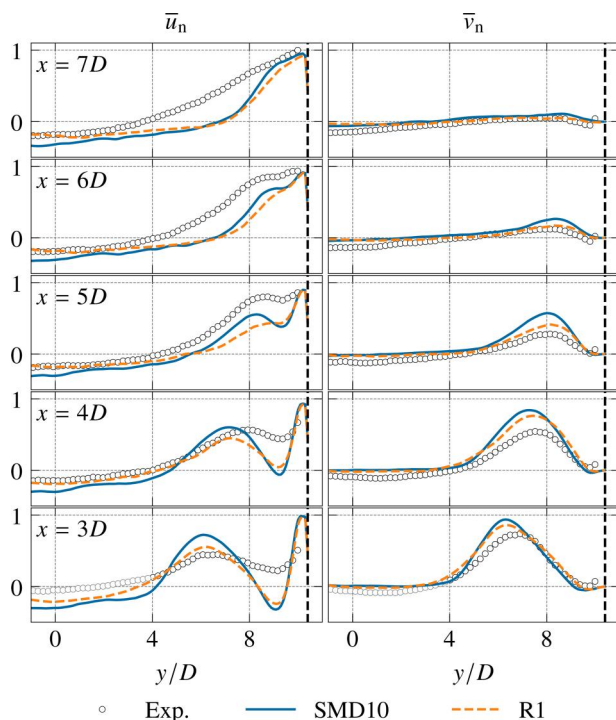


Fig. 8 Mean normalized axial and radial velocity components in the primary zone of the combustion chamber for three different spray initializations compared to experimental data. The black dashed line represents the combustor wall.

both CFD and experiments. While the CFD accurately captures the location of local maxima for both velocity components, deviations in absolute values are noted. This observation indicates that the swirled flame's opening angle is well-represented. While slight variations in the magnitude and width of the local maxima are observed with different spray initializations, the global flow characteristics in the primary zone remain unaffected, suggesting that the spray dynamics have minimal impact on the global flow fields. This consistent behavior is noted across all other spray initialization tested, which are omitted in the figure for clarity. Although minor differences in the magnitude and the width of local maxima are observed between different spray initializations, the global flow characteristic in the primary zone is not changed. In particular, the flow field in the injector (not shown in Fig. 8) used to extract the SPH-boundary conditions remains unchanged for all initialization. It is, therefore, concluded that the spray has no major influence on the flow field.

The flame position is validated by comparing OH* chemiluminescence from the experiments with the mean heat release rate of the CFD used as an indicator of the reaction zone. For the deconvolution of the line-of-sight measurements, an axis-symmetrical flow field is assumed. Although the flow in the rectangular combustion chamber does not match these criteria in all regions, the asymmetry primarily affects regions near the combustor walls and further downstream of the fuel injector. Near the fuel injector—the region of interest for OH* measurements—the flow field can be assumed axis-symmetrical. For a qualitative comparison, the experimental data and the simulation data are normalized with the local maximum value. The normalized Intensity I for two different spray initializations and the experiment is shown in Fig. 9. It has to be noted that the regions of low chemiluminescence at low radial and axial positions in the experiment are caused by artifacts of the deconvolution, e.g., the absorption of OH* signal by the liquid fuel spray, and therefore have to be excluded from any interpretation [12]. In all simulations, the highest values are found close to the fuel injector at $r = 4D$, similar to the experiment, and no significant differences are observed between the shown spray initializations. This observation

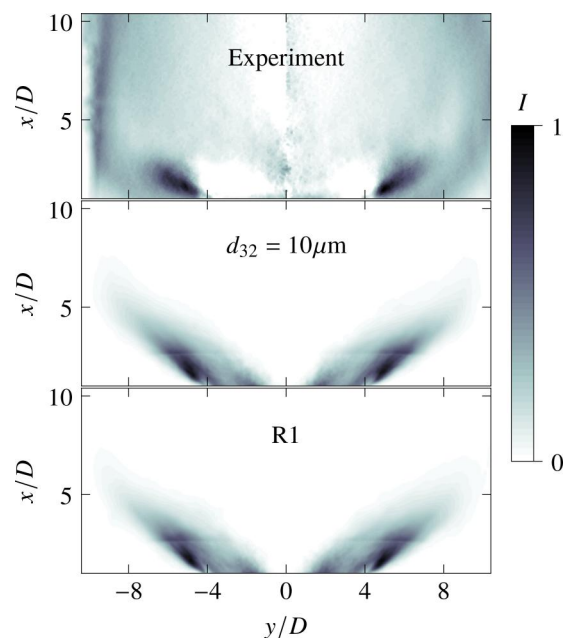


Fig. 9 Contour of the normalized deconvoluted OH* signal and the normalized heat release rate from the CFD for the flame position for two different spray initialization

also holds for the initializations SMD34, R3, and R5, omitted in the figure for clarity. It is concluded that the simulation can correctly predict the flame position and that the applied LES setup is suitable for predicting the combustion process at realistic operating conditions. A comparison of the mass flows in the different passages of the fuel injector from the initial RANS simulation with the LES results shows a maximum deviation of 10%. Therefore, and since different spray initializations have no significant influence, the iterative process depicted in Fig. 3 is not required for the current setup, and the initial SPH is sufficient to characterize the primary spray breakup.

5.2 Role of Spray Initialization in Predicting Soot Formation. To assess the impact of the fuel initialization on soot predictions, the results of all applied spray initializations (SMD10, SMD34, R1, R3, R5) are compared to LII measurements of the soot volume fraction f_v . The mean normalized soot volume fraction $f_{v,n}$ of all LES and the measurement are shown in Fig. 10. The local maximum value of all six data sets is used for normalization. All studied cases follow the same trend, with the highest f_v found in the flame branches of the primary zone. f_v increases rapidly in the vicinity of the injector at a radial position of around $3D$ and decreases further downstream. In the LES, the distance between the two soot branches is slightly larger than in the experiment. This difference is attributed to differences in the predicted fuel-air mixture. No soot is found in the central recirculation zone. A small asymmetry between the flame branches, with slightly higher values on the left, is observed and attributed to the combustor design. The swirled flame in the rectangular chamber and dual-sided secondary air injection create an inherently asymmetric flow field. When comparing the different spray initialization approaches, SMD34 and R1 significantly overpredict the magnitude of soot volume fraction in the primary zone. With SMD10, corresponding to a distribution after secondary spray breakup, soot prediction is additionally increased by a factor of two. In contrast, the cases where additional information about radial distributions are considered (R3 and R5) predict a soot distribution similar to the experiment, with R5 predicting slightly higher absolute values than R3.

For a better understanding of the differences in soot formation between the different initializations, the local mixture formation is investigated. Since first soot particles are formed through nucleation

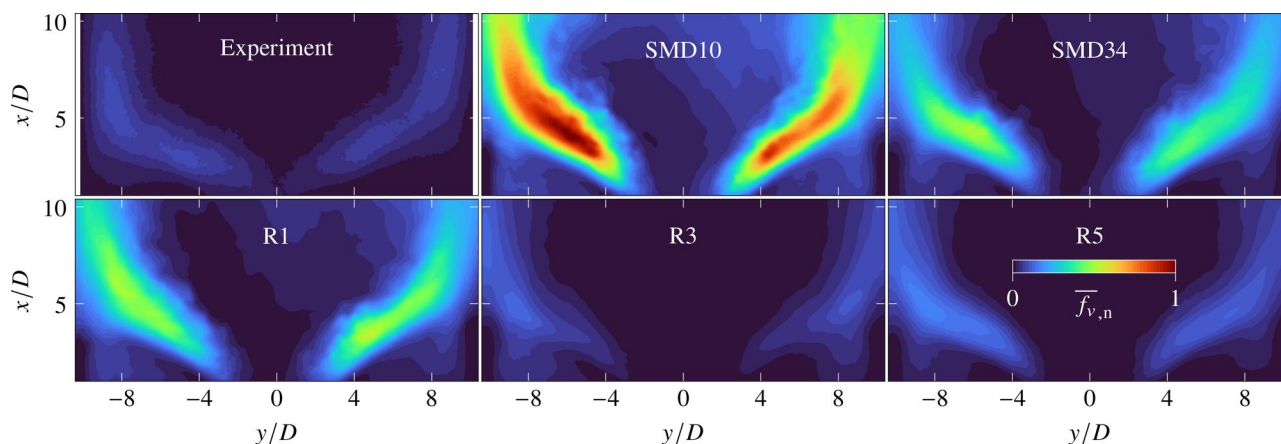


Fig. 10 Comparison of the normalized mean soot volume fraction for all applied spray initialization with experimental data on the center plane of the primary zone. The local maximum value of all six data sets is used for the normalization.

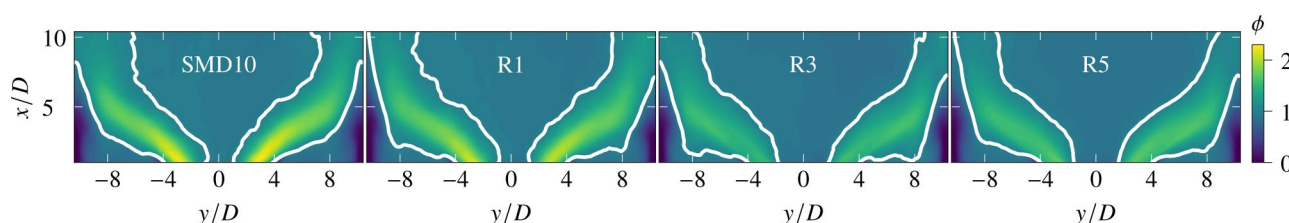


Fig. 11 Comparison of the mean local equivalence ratio for different spray initializations. The white line represents the stoichiometric mixture fraction isoline.

of polycyclic aromatic hydrocarbons (PAHs) and condensation of PAHs on soot particles further increases the soot volume fraction, soot formation is directly dependent on the mixture. Figure 11 displays the local equivalence ratio ϕ in the primary zone, with the SMD34 result omitted for clarity due to its similarity to R1. The shape of the rich zone between the two white lines remains consistent across the four simulations; however, increasing the number of radial initialization positions reduces the local maximum near the injector significantly, correlating with the mean \bar{f}_v . The highest local equivalence ratio exceeds $\phi = 2$ for $d_{32} = 10 \mu\text{m}$ and decreases to around 1.5 for the cases R3 and R5. Since the smallest initialized spray droplets are evaporated quickly, sampling the spray droplet data at a single location leads to a high fuel concentration in the region near the injector. Adding detailed information from the SPH simulation by sampling the data over multiple radial positions has a spreading effect on the fuel spray. This subsequently leads to leaner local mixtures and, therefore, fewer PAHs. The even higher mixture fraction observed for SMD10 is explained by the assumption of the distribution after secondary breakup with significantly smaller spray droplets, see Fig. 5, initialized at the same axial distance l from the prefilmer edge. This again leads to the fast evaporation of fuel spray droplets in a confined area and an increased local mixture fraction. Sampling the initialization of the fuel spray over different radial positions derived from the SPH simulations, on the other hand, leads to improved mixing of the fuel and oxidizer with leaner mixtures and decreased formation of soot precursors. These results show the importance of accurate knowledge of not only the droplet size distribution but also starting positions and velocities for predictive simulation of the mixing behavior in the combustion chamber. Since only minor differences in the soot volume fraction and equivalence ratio are observed between the results of R3 and R5, three radial positions for the spray initialization are used in the following of this study.

5.3 Impact of the Operating Conditions on Spray Dynamics and Soot Interactions. As changes in the operating conditions generally come along with changes of the flow through the injector,

different spray characteristics are to be expected. To understand which changes are important to consider in the spray modeling for emission predictions, the operating condition of the combustion chamber is varied by decreasing the fuel mass flow \dot{m}_f for the cases B–D, see Table 1. The normalized cumulative volume-based spray PSDs for all four operating points are shown in Fig. 12. All distributions follow a similar trend. However, PSD_B exhibits a shift towards larger droplets. In the first step, the same spray droplet distribution (PSD_A), corresponding to case A, is applied for all four operating points. To study the influence of the operating point-specific PSD, the corresponding distributions PSD_X are applied in a second step.

The resulting mean soot volume fractions normalized with the overall local maximum in the primary zone for all simulations and experiments are shown in Fig. 13. As expected, the experiments show that the total amount of soot is decreased with decreasing \dot{m}_f due to overall leaner mixtures. While \bar{f}_v is also reduced in the CFD when using the same PSD for all operating points, and the soot distribution zones resemble those in the experiment, the trend no longer aligns with the experimental results. Soot is slightly

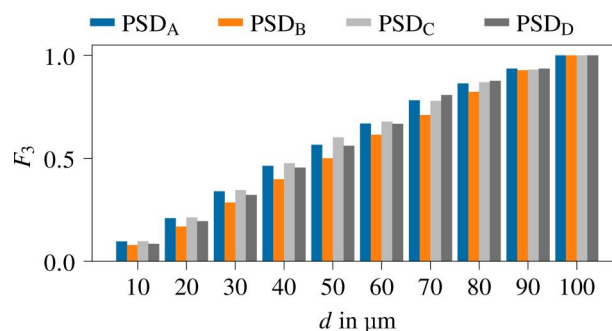


Fig. 12 Normalized cumulative volume based spray particle size distribution sampled from SPH simulations for all four studied operating conditions

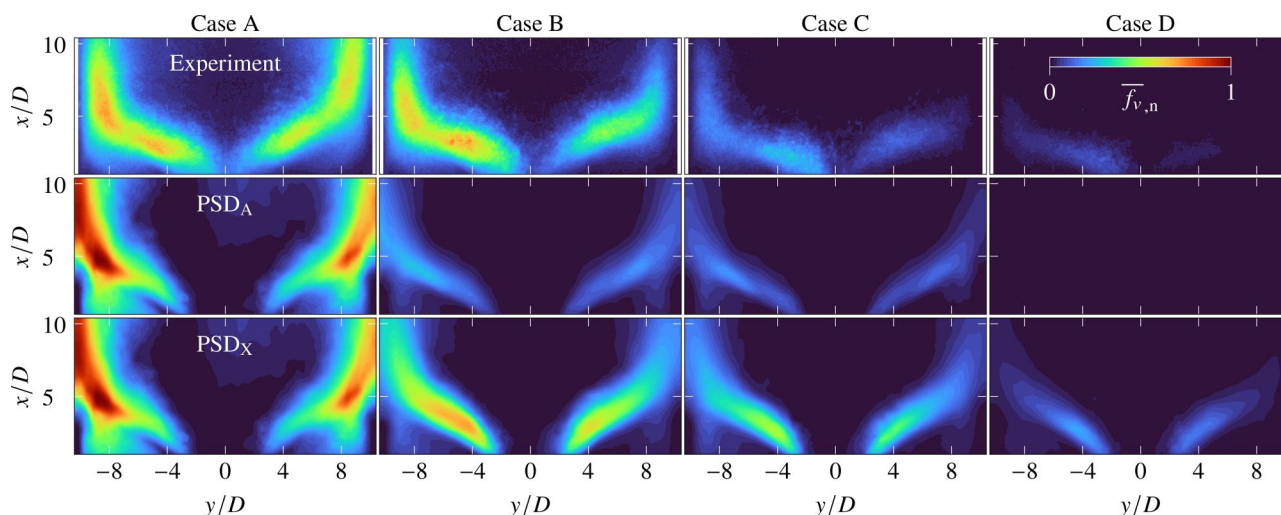


Fig. 13 Mean normalized soot volume fraction in the primary zone of the combustor compared to the experimental data for different fuel mass flows. The first row represents the experimental data, the second row the CFD results with the same spray PSD applied for all fuel mass flows while the bottom row shows the results when using the spray PSD corresponding to the specific fuel mass flow.

overpredicted for the highest fuel mass flow. Although soot is decreased when lowering m_f , it is now lower than in the experiments for cases B and C, and for the lowest fuel mass flow, no soot is visible anymore. These results are improved significantly by applying the PSD corresponding to the respective operating point, as seen in the bottom line of Fig. 13. The LES, now in line with the experimental data, can accurately predict the trend of decreasing soot volume fraction between the different operating points. The importance of the applied distribution is explained by comparing the case-specific droplet distributions in Fig. 6. Applying PSD_A with the largest radial spread of the droplets to the other cases leads to locally leaner mixtures and, therefore, underprediction of soot formation. A possible reason for the overprediction of soot in the simulation is uncertainties regarding the applied fuel. While the low aromatic fuel D70 is applied in the experiment, a kerosene surrogate is used for the simulations. This difference might result in potential differences in the gas mixture.

The variation of the fuel mass flow has shown that, since the spray breakup varies over the operating range, initializing the respective distribution is indispensable to capture the correct mixing trends and, consequently, the correct soot prediction.

6 Conclusion

This combined numerical and experimental study has investigated a single-sector combustor with an aero-engine fuel injector operating at high pressures and preheating temperatures. The focus of this work is to elucidate the impact of liquid fuel spray on soot emissions. A segregated approach utilizing specialized solvers for fuel breakup and the reacting flow allows the simulation of the entire cause-and-effect chain—from primary breakup to soot formation. Spray characteristics sampled from highly resolved SPH simulations of the fuel breakup were used as initialization for the liquid fuel spray in the LES. By applying different initialization strategies, the influence of the fuel spray boundary condition was studied, and simulation results were validated against experimental data. Key findings include:

- The applied numerical setup accurately predicts velocities and flame position.
- Variations in spray boundary condition have only minor effects on the global flow characteristics.
- Local mixture formation is highly sensitive to spray initialization, directly influencing the prediction of soot formation.

The results underscore that global flow quantities, such as velocity, are insufficient indicators of the mixture distribution. Including the radial distribution of the fuel spray in the LES resulted

in locally leaner mixtures and reduced soot formation, improving alignment between simulation results and experiments. Extending the study to additional operating conditions further highlighted the necessity of accurate spray PSD information for replicating experimental trends.

This single-sector study demonstrates the importance of capturing the complete cause-and-effect chain, from primary atomization to soot formation. Establishing flexible interfaces between critical subprocesses ensures that they can be addressed sequentially rather than requiring simultaneous simulations. This represents a significant advancement for the LES of realistic aero-engine combustors.

Acknowledgment

The authors gratefully acknowledge the computing time provided to them on the high-performance computer Lichtenberg II at the NHR Centers NHR4CES at TU Darmstadt for the LES. The authors acknowledge support by the state of Baden-Württemberg through bwHPC for the SPH simulations. The authors would like to express their gratitude to Johannes Heinze and Eggert Magens for their valuable assistance during the experimental test campaign.

Funding Data

- German Federal Ministry for Economic Affairs and Energy under the Federal Aeronautical Research Program (LuFo V) (Grant No. 20T1516; Funder ID: 10.13039/501100006360).
- German Federal Ministry for Economic Affairs and Energy under the Federal Aeronautical Research Program (LuFo VI, Call 2) (Grant No. 20D2102C; Funder ID: 10.13039/501100006360).

Data Availability Statement

The datasets generated and supporting the findings of this article are obtainable from the corresponding author upon reasonable request.

References

- [1] Valencia, S., Ruiz, S., Manrique, J., Celis, C., and Figueira Da Silva, L. F., 2021, "Soot Modeling in Turbulent Diffusion Flames: Review and Prospects," *J. Braz. Soc. Mech. Sci. Eng.*, **43**(4), p. 219.
- [2] Leung, K. M., Lindstedt, R. P., and Jones, W. P., 1991, "A Simplified Reaction Mechanism for Soot Formation in Nonpremixed Flames," *Combust. Flame*, **87**(3–4), pp. 289–305.
- [3] Mueller, M. E., and Pitsch, H., 2013, "Large Eddy Simulation of Soot Evolution in an Aircraft Combustor," *Phys. Fluids*, **25**(11), p. 110812.

- [4] Koob, P., Ferraro, F., Nicolai, H., Eggels, R. L. G. M., Stauffer, M., and Hasse, C., 2024, "Large Eddy Simulation of Soot Formation in a Real Aero-Engine Combustor Using Tabulated Chemistry and a Quadrature-Based Method of Moments," *ASME J. Eng. Gas Turbines Power*, **146**(1), p. 011015.
- [5] Eigentler, F., Gerlinger, P., and Eggels, R., 2022, "Soot CFD Simulation of a Real Aero Engine Combustor," *AIAA* Paper No. 2022-0489.
- [6] Rolls-Royce plc, ed., 2015, *The jet engine*, Wiley, Chichester, West Sussex.
- [7] Braun, S., Wieth, L., Holz, S., Dauch, T. F., Keller, M. C., Chaussonnet, G., Geppert, S., Koch, R., and Bauer, H.-J., 2019, "Numerical Prediction of Air-Assisted Primary Atomization Using Smoothed Particle Hydrodynamics," *Int. J. Multiphase Flow*, **114**, pp. 303–315.
- [8] Dauch, T. F., Braun, S., Wieth, L., Chaussonnet, G., Keller, M. C., Koch, R., and Bauer, H.-J., 2017, "Computational Prediction of Primary Breakup in Fuel Spray Nozzles for Aero-Engine Combustors," *ILASS-Europe 2017. 28th Conference on Liquid Atomization and Spray Systems*, Valencia, Spain, Sept. 6–8, pp. 1–8.
- [9] Warnke, K., Sadiki, A., Stauffer, M., Hasse, C., and Janicka, J., 2020, "Towards Primary Breakup Simulation of a Complete Aircraft Nozzle at Realistic Aircraft Conditions," *ASME* Paper No. GT2020-14597.
- [10] Rizk, N. K., and Lefebvre, A. H., 1985, "Drop-Size Distribution Characteristics of Spill-Return Atomizers," *J. Propul. Power*, **1**(1), pp. 16–22.
- [11] Okrashevski, M., Mesquita, L. C. C., Koch, R., Mastorakos, E., and Bauer, H.-J., 2023, "A Numerical Study of Aero Engine Sub-idle Operation: From a Realistic Representation of Spray Injection to Detailed Chemistry LES-CMC," *Flow, Turbul. Combust.*, **111**(2), pp. 493–530.
- [12] Soworka, T., Behrendt, T., Hassa, C., Heinze, J., Magens, E., Schroll, M., di Mare, F., Ballantyne, S., and Gregory, J., 2019, "Experimental Investigation of a RQL Burner With Jet in Cross Flow Fuel Injection: Characterization of the Reacting Flow Field at Realistic Operating Conditions," *ASME* Paper No. GT2019-91244.
- [13] Hassa, C., Magens, E., Voigt, L., Diers, O., Otterpohl, I., and Heinze, J., 2020, "Soot Formation and Emission From Jet A-1 and a 30% HEFA Blend in a Multisector Combustor at Realistic Operating Conditions," *ASME* Paper No. GT2020-14462.
- [14] Meier, U., Heinze, J., Magens, E., Schroll, M., Hassa, C., Bake, S., and Doerr, T., 2015, "Optically Accessible Multisector Combustor: Application and Challenges of Laser Techniques at Realistic Operating Conditions," *ASME* Paper No. GT2015-43391.
- [15] Schroll, M., Klinger, J., Lange, L., and Willert, C., 2013, "Particle Image Velocimetry of Highly Luminescent, Pressurized Combustion Flows of Aero Engine Combustors," *10th International Symposium on Particle Image Velocimetry (PIV13)*, Delft, Netherlands, July 2–4, pp. 1–9.
- [16] Axelsson, B., Collin, R., and Bengtsson, P., 2001, "Laser-Induced Incandescence for Soot Particle Size and Volume Fraction Measurements Using On-Line Extinction Calibration," *Appl. Phys. B*, **72**(3), pp. 367–372.
- [17] Anand, M. S., Eggels, R., Stauffer, M., Zedda, M., and Zhu, J., 2014, "An Advanced Unstructured-Grid Finite Volume Design System for Gas Turbine Combustion Analysis," *ASME* Paper No. GTINDIA2013-3537.
- [18] Jasak, H., Weller, H., and Gosman, A., 1999, "High Resolution NVD Differencing Scheme for Arbitrarily Unstructured Meshes," *Int. J. Numer. Methods Fluids*, **31**(2), pp. 431–449.
- [19] Nicoud, F., Toda, H. B., Cabrit, O., Bose, S., and Lee, J., 2011, "Using Singular Values to Build a Subgrid-Scale Model for Large Eddy Simulations," *Phys. Fluids*, **23**(8), p. 085106.
- [20] van Oijen, J. A., and de Goey, L. P., 2000, "Modelling of Premixed Laminar Flames Using Flamelet-Generated Manifolds," *Combust. Sci. Technol.*, **161**(1), pp. 113–137.
- [21] Ramirez Hernandez, A., Kathrotia, T., Methling, T., Braun-Unkloff, M., and Riedel, U., 2023, "An Upgraded Chemical Kinetic Mechanism for Iso-Octane Oxidation: Prediction of Polyaromatics Formation in Laminar Counterflow Diffusion Flames," *ASME J. Eng. Gas Turbines Power*, **145**(6), p. 061006.
- [22] Koob, P., Nicolai, H., Schmitz, R., and Hasse, C., 2024, "Analysis of Potential Soot Breakthrough During Oxidation at Aero-Engine Relevant Conditions," *Proc. Combust. Inst.*, **40**(1–4), p. 105672.
- [23] Eggels, R. L. G. M., 2018, "The Application of Combustion LES Within Industry," in *Direct and Large-Eddy Simulation X*, D. G. Grigoriadis, B. J. Geurts, H. Kuerten, J. Fröhlich, and V. Armenio, eds., Springer International Publishing, Cham, pp. 3–13.
- [24] Poinso, T., and Veynante, D., 2005, *Theoretical and numerical combustion*, 2nd ed., Edwards, Philadelphia, PA.
- [25] Salenbauch, S., Hasse, C., Vanni, M., and Marchisio, D. L., 2019, "A Numerically Robust Method of Moments With Number Density Function Reconstruction and its Application to Soot Formation, Growth and Oxidation," *J. Aerosol Sci.*, **128**, pp. 34–49.
- [26] Mueller, M. E., and Pitsch, H., 2012, "LES Model for Sooting Turbulent Nonpremixed Flames," *Combust. Flame*, **159**(6), pp. 2166–2180.
- [27] Balthasar, M., Mauss, F., Pfitzner, M., and Mack, A., 2002, "Implementation and Validation of a New Soot Model and Application to Aeroengine Combustors," *ASME J. Eng. Gas Turbines Power*, **124**(1), pp. 66–74.
- [28] Brocklehurst, H. T., Priddin, C. H., and Moss, J. B., 1997, "Soot Predictions Within an Aero Gas Turbine Combustion Chamber," *ASME* Paper No. 97-GT-148.
- [29] Thari, A., 2022, "Asynchronous Task Based Eulerian-Lagrangian Parallel Solver for Large Scale Combustion Applications," Ph.D. thesis, Loughborough University, Loughborough, England.
- [30] Celik, I. B., Cehreli, Z. N., and Yavuz, I., 2005, "Index of Resolution Quality for Large Eddy Simulations," *ASME J. Fluids Eng.*, **127**(5), pp. 949–958.
- [31] Monaghan, J. J., 2005, "Smoothed Particle Hydrodynamics," *Rep. Prog. Phys.*, **68**(8), pp. 1703–1759.
- [32] Braun, S., Koch, R., and Bauer, H.-J., 2016, "Smoothed Particle Hydrodynamics for Numerical Predictions of Primary Atomization," in *High Performance Computing in Science and Engineering '16*, W. E. Nagel, D. H. Kröner, and M. M. Resch, eds., Springer International Publishing, Cham, pp. 321–336.
- [33] Chaussonnet, G., Braun, S., Dauch, T., Keller, M., Sängler, A., Jakobs, T., Koch, R., Kolb, T., and Bauer, H.-J., 2019, "Toward the Development of a Virtual Spray Test-Rig Using The Smoothed Particle Hydrodynamics Method," *Comput. Fluids*, **180**, pp. 68–81.
- [34] Liu, M. B., and Liu, G. R., 2010, "Smoothed Particle Hydrodynamics (SPH): an Overview and Recent Developments," *Arch. Comput. Methods Eng.*, **17**(1), pp. 25–76.
- [35] Cole, R., 1948, *Underwater Explosions* (Dover Books on Engineering and Engineering Physics), Dover Publications, New York.
- [36] Dauch, T., Braun, S., Wieth, L., Chaussonnet, G., Keller, M., Koch, R., and Bauer, H.-J., 2016, "Computation of Liquid Fuel Atomization and Mixing by Means of the SPH Method: Application to a Jet Engine Fuel Nozzle," *ASME* Paper No. GT2016-56023.
- [37] Dauch, T. F., Ates, C., Rapp, T., Keller, M. C., Chaussonnet, G., Kaden, J., Okrashevski, M., Koch, R., Dachsbacher, C., and Bauer, H.-J., 2019, "Analyzing the Interaction of Vortex and Gas-Liquid Interface Dynamics in Fuel Spray Nozzles by Means of Lagrangian-Coherent Structures (2D)," *Energies*, **12**(13), p. 2552.
- [38] Schmehl, R., 2002, "Advanced Modeling of Droplet Deformation and Breakup for CFD Analysis of Mixture Preparation," *18th Annual Conference on Liquid Atomization and Spray Systems (ILASS2002)*, Zaragoza, Spain, Sept. 9–11, pp. 1–8.
- [39] Chin, J. S., and Lefebvre, A. H., 1983, "Steady-State Evaporation Characteristics of Hydrocarbon Fuel Drops," *AIAA J.*, **21**(10), pp. 1437–1443.